The Removal of Phosphate from Aqueous Solutions by Sepiolite/ZrO_2 Composites: Adsorption Behavior and Mechanism

Željka Milovanović , Slavica Lazarević * , Ivona Janković-Častvan , Željko Radovanović , Slobodan Cvetković , Djordje Janaćković , Rada Petrović

Posted Date: 6 June 2023

doi: 10.20944/preprints202306.0365.v1

Keywords: Sepiolite; Zr-propoxide functionalization; Phosphate adsorption; Adsorption kinetics; XPS analysis

Article

The Removal of Phosphate from Aqueous Solutions by Sepiolite/ZrO_2 Composites: Adsorption Behavior and Mechanism

Željka Milovanović [1], Slavica Lazarević [2]*, Ivona Janković-Častvan [2], Željko Radovanović [3], Slobodan Cvetković [1], Đorđe Janaćković [2] and Rada Petrović [2]

[1] University of Belgrade, Institute of Chemistry, Technology and Metallurgy, National Institute of the Republic of Serbia, Department of Ecology and Technoeconomics, Njegoševa 12, 11001 Belgrde, Serbia
[2] University of Belgrade, Faculty of Technology and Metallurgy, Karnegijeva 4, 11000 Belgrade, Serbia
[3] Innovation Center of the Faculty of Technology and Metallurgy, Karnegijeva 4, 11000 Belgrade, Serbia
* Correspondence: slazarevic@tmf.bg.ac.rs.

Abstract: The sepiolite/ZrO_2 composites were prepared by sepiolite (Sep) modification with zirconium propoxide in toluene, at room temperature for 24 h (Sep –ZrI) or 95 °C for 4h (sample Sep –ZrII). The efficiency of the obtained adsorbents for the removal of phosphate from aqueous solutions at initial pH = 4 and pH = 8, was investigated. Characterization of the samples showed that higher temperature of synthesis for shorter time provided slightly higher content of amorphous Zr-phase, which was deposited on sepiolite fibers as a thin layer and agglomerated nanoparticles. Compared to Sep, the composites had lower point of zero charge and higher specific surface area and pore volume. The adsorption kinetics follows the pseudo second-order model. The adsorption capacities of the composites were approximately the same at both initial pH and higher at initial pH = 4 than at pH = 8. The XPS and ATR-FTIR of Sep-ZrI before and after adsorption identified the formation of inner-sphere complexes as the mechanism of phosphate adsorption. The slow release during desorption with NaOH solution confirmed strong bonds of phosphates with the surface of the composites.

Keywords: Sepiolite; Zr-propoxide functionalization; Phosphate adsorption; Adsorption kinetics; XPS analysis

1. Introduction

Phosphorus (P) is one of the essential elements for organisms in aquatic environments, but high concentrations of P as a result of excessive use of fertilizers, discharging of urban and industrial wastewaters, etc. cause the process of eutrophication [1]. During the eutrophication, algae blooms can occur, which leads over time to the high number of dead organisms, which are decomposed by saprophytes, where they use oxygen [2]. As a result, the concentration of oxygen in the water body decreases and thus there is suffocation and mass death of aquatic organisms, which need oxygen for the process of respiration [1,3–5]. In this regard, the methods that can effectively remove P from water are being investigated [5].

Various technologies have been used to remove excess P from water and wastewater, among which biological processes and chemical precipitation are most commonly used [2,5]. However, these methods have several drawbacks: relatively low efficiency, waste sludge production and high operating costs [5,6]. On the other hand, adsorption has proven to be an efficient, simple and one of the most economical methods for removing P from water [1,6–8], but only if low-cost adsorbents with high adsorption capacity are used.

So far, various low-cost natural or waste materials have been tested as adsorbents for P, but their adsorption capacities are very low due to low specific surface area, low affinity of functional groups and/or negative surface charge, having in mind that P is present in the aquatic environment as

 doi:10.20944/preprints202306.0365.v1

phosphate anions (PO_4^{3-}, HPO_4^{2-} or $H_2PO_4^-$, depending on pH) [9]. Therefore, many metal oxides/hydroxides have been used in phosphate adsorption studies considering their preferable phosphate capture through specific adsorption by Lewis acid-base interactions [10]. Due to remarkable selectivity to phosphate ions and high chemical stability under acidic and basic conditions, zirconium oxide/hydroxide has great potential to immobilize phosphate from water [11,12]. In order to prevent agglomeration and provide high content of active species for phosphate adsorption, zirconium oxide/hydroxide nanoparticles have been dispersed on different low-cost supports with high surface area and appropriate porosity, such as: zeolite [13,14], bentonite [15–17], mesoporous SiO_2 [18], polymeric anion exchanger [19,20], chitosan [21], *etc.*

To the best of our knowledge, the natural fibrous clay mineral sepiolite has not been used up to now as the support for zirconium oxide/hydroxide particles to prepare adsorbent for phosphates. Sepiolite is a hydrated magnesium silicate with the ideal formula $Si_{12}Mg_8O_{30}(OH)_4(OH_2)_4 \cdot 8H_2O$, whose structure is similar to those of other 2:1 trioctahedral silicates, such as talc, but it has discontinuities and inversion of the silica sheets, which give rise to structural tunnels and blocks [22]. The tunnels are filled by zeolitic H_2O molecules and exchangeable cations. Due to the discontinuities and layer-chain structure, silanol groups (Si-OH) are presented on the external surface of sepiolite and structural OH_2 molecules complete the coordination of octahedral cations. Sepiolite has the highest surface area of all the clay minerals, not only as a result of the small size of its particles, but also because of its fibrous morphology and intracrystalline porosity. On the other hand, the specific surface area is decreased due to strong hydrogen bonding and Van der Waals' interactions between the fibers, causing formation bundles of fibres. Due to the negative surface charge, sepiolite has a high adsorption capacity for cations but a very low affinity for anions.

In general, the deposition of ZrO_2 on supports has been carried out in various ways, but usually using $ZrOCl_2 \cdot 8H_2O$ dissolved in water [13,23–26] or $Zr(OC_3H_7)_4$ dissolved in toluene [18,27]. When $ZrOCl_2 \cdot 8H_2O$ has been used, ZrO_2 was deposited mostly as nano-particles and $Zr(OC_3H_7)_4$ dissolved in toluene was used to provide a molecular level dispersion of ZrO_2 functionality giving rise to high surface exposure of adsorption site and thus high adsorption capacity for phosphate [18,27]. During modification of sepiolite with $Zr(OC_3H_7)_4$, the alkoxy-groups of the $Zr(OC_3H_7)_4$ should react with silanol groups on the sepiolite surface, forming Si–O–Zr covalent bonds. By subsequent hydrolysis, the remaining alkoxide groups attached to covalently bound zirconia are converted into Zr-OH group.

Therefore, in this study, new adsorbents for phosphates were synthesized by adding $Zr(OC_3H_7)_4$ into sepiolite suspension in toluene, under inert atmosphere, and the suspension was mixed: i) at room temperature for 24 h, similar to the case of silane grafting onto sepiolite [28], or ii) at 95 °C for 4 h, similar to the case of zirconia-functionalization of graphite oxide [27] and SBA-15 [18]. The influence of the synthesis conditions on the properties of Zr-sepiolites and adsorption performances was investigated. The effects of pH, contact time and initial concentration on phosphate adsorption were examined and the mechanisms of the adsorption are discussed.

2. Materials and Methods

2.1. Materials

The used natural sepiolite (Sep) came from Andrici (Serbia). Characterization of the sample has been performed and reported previously [29].

Zirconium(IV) propoxide ($Zr(OC_3H_7)_4$) (70% in propanol solution) was purchased from Fluka and used as received without further purification. Toluene (Toluene P.A., Lach:ner) was used for the modification process. All other chemical reagents such as KNO_3, NaOH, HCl, were of analytical grade and used as received. Potassium dihydrogen phosphate anhydrous KH_2PO_4 (p.a. Lach:ner) was used to prepare the phosphate stock solution. All solutions were prepared with high purity water (18 MΩ/cm).

2.2. Sepiolite Modification with Zirconium(IV) Propoxide

 doi:10.20944/preprints202306.0365.v1

The Sep was modified in a stream of nitrogen, on a magnetic stirrer at a ratio of 10 g of sepiolite and 250 cm^3 of toluene, for 30 min, after which 13.5 cm^3 of $Zr(OC_3H_7)_4$ was added and left in a stream of nitrogen at room temperature for 24 h, in one case (sample Sep-ZrI) or at 95 °C for 4 h, in other case (sample Sep-ZrII). The obtained samples were then centrifuged, and washed with toluene, ethanol and deionized water. The solids thus obtained were oven dried at 110 °C for 24 hours.

2.3. Characterization of the Samples

The particles morphology of the samples was observed by a Tescan MIRA3 field emission gun scanning electron microscope (FESEM), with electron energies of 20 kV in a high vacuum. The samples were sputter-coated with an Au alloy to ensure conductivity. Energy-dispersive X-ray spectroscopy of the samples was performed on the device Jeol JSM 5800 Sem (Oxford Link Isis 300). X-ray diffraction (XRD) analysis of the samples was realized with an ITAL STRUCTURES APD 2000 diffractometer using CuKα radiation, in the 2Θ angle range from 3º to 50º, with a 0.02º step. ATR-FTIR spectra of the samples were recorded in absorbance mode using a Nicolet™ iS™ 10 FTIR Spectrometer (Thermo Fisher SCIENTIFIC) with Smart iTR™ ATR Sampling accessories, within a range of 4000–400 cm^{-1}, at a resolution of 4 cm^{-1} and in 20 scan mode. Thermal behavior was determined by simultaneous TG–DTA (Setsys, SETARAM Instrumentation, Caluire, France) up to 1000 °C with a heating rate of 5°/min in air flow, in an Al_2O_3 pan.

The specific surface area (S_{BET}) and pore size distribution of the samples were determined using nitrogen adsorption–desorption isotherms obtained by a Micrometrics ASAP 2020 instrument. Prior to adsorption measurements, the samples were degassed at 150 °C for 10 h under reduced pressure. The S_{BET} of the samples was calculated from the linear part of the nitrogen adsorption isotherm according to the method BET [30]. The volume of the mesopores (V_{meso}) and pore size distribution were analyzed according to the Barrett, Joyner and Halenda BJH method [31], using the desorption isotherm. The volume of the micropores (V_{micro}) was calculated according to the α-plot analysis [32].

The point of zero charge (pH_{pzc}) was determined by the batch equilibration method [33], in KNO_3 solutions with a concentration of 0.1, 0.01 or 0.001 mol/dm^3. The initial pH values (pH_i) of KNO_3 solutions (20 cm^3) were adjusted by adding of 1 mol/dm^3 HNO_3 or 0.1 mol/dm^3 KOH, in the pH range from 3 to 10. Then 0.02 g of the sample was added to the solution and kept under constant stirring for 24 h at 25 °C. Finally, the samples were filtered and the pH values of the filtrates (pH_f) were measured. The pH_{pzc} was obtained from the dependence of pH_f on pH_i as the pH where a plateau appears on the curve pH_f vs. pH_i [29].

XPS analysis of the samples Sep-ZrI before and after adsorption was carried out on SPECS Systems with XP50M X-ray source for Focus 500 and PHOIBOS 100 energy analyzer using a monochromatic Al Kα X-ray source (1486.74 eV) at 12.5 kV and 12 mA. The sample was fixed onto an adhesive copper foil to provide strong mechanical attachment and good electrical contact. Survey XPS spectrum (0–1000 eV BE) was recorded with a constant pass energy of 40 eV, energy step of 0.5 eV, and the dwell time of 0.2 s, while high resolution XPS spectra of the corresponding lines were taken with a pass energy of 20 eV, energy step of 0.1 eV and a dwell time of 2 s. The XPS spectra were collected by SpecsLab data analysis software, and analyzed using the CasaXPS software package. A standard Shirley background is used for all sample spectra.

2.4. Adsorption experiments

The adsorption experiments were carried out in a batch procedure in a thermostatic water bath with shaking at a temperature of 25 ± 1 °C. After separation of the adsorbent, the concentration of phosphate ions was determined by UV/Vis spectroscopy Lambda 25/35/45 Perkin Elmer, at 880 nm.

The effect of pH_i on phosphate adsorption was investigated by adjusting a phosphate solution with an initial P concentration of 20 mg/dm^3 to different pH values from 3 to 10 and shaking 0.02 g of the Sep-ZrI or Sep-ZrII in 20 cm^3 of phosphate solution for 24 h.

For the purpose of determining the adsorption isotherms, solutions of different P concentrations were prepared. Aliquot of 20 cm^3 of each solution was shaken for 24 h with 0.02 g of the sample. The adsorption isotherms were determined at pH_i of 4.0 ± 0.1 and 8.0 ± 0.1.

Preprints (www.preprints.org) | NOT PEER-REVIEWED | Posted: 6 June 2023 doi:10.20944/preprints202306.0365.v1

Kinetic experiments were performed at two concentrations of 5 and 20 mg P/dm^3, at pHi 4.0 ± 0.1 and 8.0 ± 0.1, for contact times ranging from 1 h to 24 h.
The adsorbed quantities of phosphates per unit mass of adsorbents (q) were calculated using Equation (1):

$$q = \frac{c_i - c_f}{m} \cdot V \quad (1)$$

where q is the adsorption capacity (mg/g); c_i is the initial phosphate concentration (mg/dm^3), c_f is the final phosphate concentration after solution shaking with the adsorbent (mg/dm^3); m is the mass of the adsorbent (g), and V is the solution volume (dm^3).

The isotherm data were fitted using Langmuir [34] and Freundlich isotherm models [35]. The kinetic data were fitted using the pseudo-first-order model [36], the pseudo-second-order kinetic model [37], and the intraparticle diffusion model [38].

2.5. Desorption

Desorption studies were performed with the samples obtained by the phosphate adsorption from a solution with a concentration of 20 mg P/dm^3 at pH$_i$ 4 ± 0.1 and 8 ± 0.1. Desorption was performed for 1–24 h by stirring 0.02 g of phosphate-loaded Sep-ZrI and Sep-ZrII (m_d) with 20 cm^3 (V_d) of 0.1 mol/dm^3 NaOH solution at 298 K. The suspensions were then filtered and the phosphate concentration in the solution, $c_{t,d,}$ was determined by UV-Vis. The quantities of phosphate desorbed per unit mass of the loaded samples, $q_{t,d}$, were calculated using the following equation:

$$q_{t,d} = \frac{c_{t,d}}{m_d} \cdot V_d \quad (2)$$

Desorption efficiency is given as a percentage of the amount of phosphate desorbed per unit mass of the Sep-ZrI or Sep-ZrII, $q_{t,d}$, to the amount of phosphate adsorbed per unit mass of the adsorbent, q_e.

3. Results and Discussion

3.1. Characterization of the Samples

EDS analysis of the samples (Table 1) showed the presence of O, Mg, and Si, as the main elements of sepiolite and Zr as a result of the modification. Iron is present as an impurity in the Sep [29]. The wt.% of Zr in the Sep-ZrII is slightly higher and the wt.% of Mg and Si are somewhat lower, indicating a slightly lower content of sepiolite, *i.e.* a higher content of ZrO_2 in the sample Sep-ZrII. Although the differences are not so big, it can be stated that the modification at a higher temperature (95 °C compared to room temperature) for a shorter time (4 h in comparison to 24 h) provided a slightly higher content of deposited Zr compounds.

Table 1. Results of EDS analysis of the Sep- ZrI and Sep- ZrII (in wt. %).

Sample	O	Mg	Si	Fe	Zr
Sep-ZrI	56.26±0.99	8.84±0.37	17.42±0.93	1.05±0.15	16.42±0.30
Sep-ZrII	57.87±3.53	7.38±0.72	14.45±1.19	0.96±0.16	19.35±2.39

Diffractograms of Sep-ZrI and Sep-ZrII (Figure 1) display peaks that are typical for the sepiolite, proving that the basic sepiolite structure was unaltered by the modification procedures [29]. The absence of other peaks in the diffractograms of Sep-ZrI and Sep-ZrII in comparison to Sep indicates the formation of amorphous zirconia compounds. The intensities of the sepiolite peaks in the diffractograms of the Sep-ZrI and Sep-ZrII are slightly lower than for Sep, which can be a consequence of a smaller content of the sepiolite due to the presence of amorphous Zr-phase.

Preprints (www.preprints.org) | NOT PEER-REVIEWED | Posted: 6 June 2023 doi:10.20944/preprints202306.0365.v1

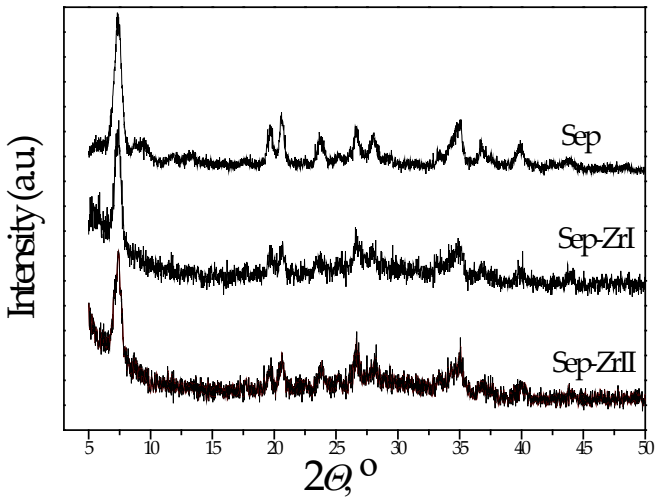

Figure 1. XRD patterns of the Sep, Sep-ZrI and Sep-ZrII.

Differential thermal analysis of the samples (Figure 2) showed peaks characteristic for sepiolite: an endothermic peak centered at about 100 °C, which is attributed to the removal of physically bound water and ethanol used in the synthesis, which is followed by weight loss (TG curve), while an exothermic peak at about 835 °C indicates sepiolite transformation to enstatite ($MgSiO_3$) and SiO_2, without the weight loss. The slightly lower intensity of the exothermic peak for Sep-ZrII indicates a slightly lower content of sepiolite in that sample, i.e. a slightly higher content of Zr compounds in comparison to Sep-ZrII, which is in accordance with the EDS results. Weight loss in the temperature range 200–800 °C corresponds to the loss of coordinated and structural (OH group) water, which should be seen as endothermic peaks at DTA curves. However, a wide exothermic peak is seen in that temperature range, which can be explained by the crystallization of the amorphous ZrO_2 in the samples [39]. The higher intensity of the peak for Sep-ZrII can be another indication of the higher content of ZrO_2 in that sample.

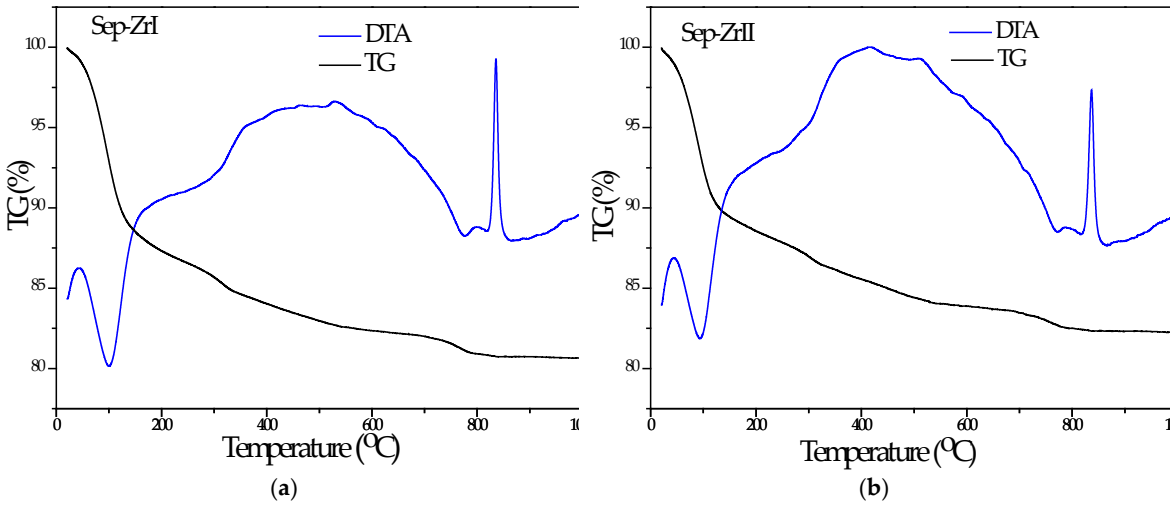

Figure 2. DTA and TGA of the samples: (**a**) Sep-ZrI and (**b**) Sep-ZrII.

The SEM micrographs of the Sep-ZrI and Sep-ZrII samples (Figure 3) show the presence of fibrous sepiolite particles and aggregates of fine spherical particles, obviously zirconium oxide/hydroxide's. Although the Zr content in the samples is approximately the same, the aggregates of Zr-based particles are seemed more abundant in Sep–ZrI than in Sep–ZrII (Figure 3). It is possible that the Zr-phase is deposited more uniformly as a thin film on the sepiolite particles in the case of Sep–ZrII, which cannot be clearly seen on SEM micrographs. The idea of the modification with $Zr(OC_3H_7)_4$ in toluene was to enable the reaction between silanol groups at the sepiolite surface with

Preprints (www.preprints.org) | NOT PEER-REVIEWED | Posted: 6 June 2023 doi:10.20944/preprints202306.0365.v1

the alkoxy group from $Zr(OC_3H_7)_4$ (grafting reaction), not to hydrolyze the alkoxide and precipitate $Zr(OH)_4$ as agglomerated particles. Taking into account the SEM micrographs (Figure 3), it can be supposed that some quantity of alkoxide was not grafted onto sepiolite, but remained adsorbed on the sepiolite surface and hydrolyzed during the samples washing after centrifugation. In that way, agglomerates of fine Zr-based particles were attached to the sepiolite fibers or bundles of fibers, giving amorphous ZrO_2 after drying. It is possible that the grafting is more pronounced at higher temperatures, so the quantity of the remaining alkoxide was lower in the case of Sep-ZrII and thus the amount of agglomerates.

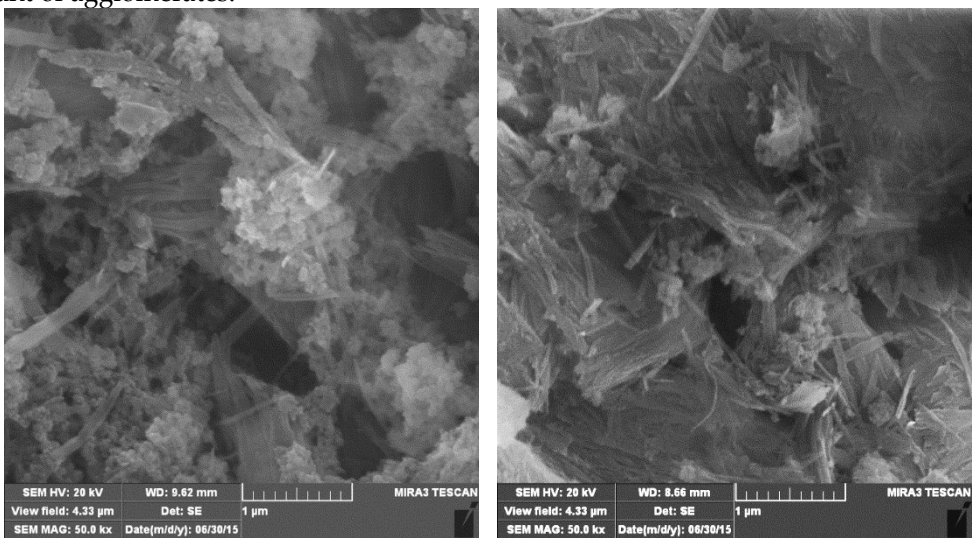

(**a**) (**b**)

Figure 3. SEM micrographs of: (**a**) Sep-ZrI; (**b**) Sep-ZrII.

The calculated S_{BET}, V_{micro}, V_{meso}, the overall pore volume (V_{total}), the mesopore size at which the pore size distribution achieves its maximum (D_{max}) and the average mesopore diameter ($D_{average}$) are summarized in Table 2.

Table 2. The textural characteristics of the Sep-ZrI and Sep-ZrII in comparison to Sep.

Sample	S_{BET}, m^2/g	V_{total}, m^3/g	V_{meso}, cm^3/g	V_{micro}, cm^3/g	D_{mean}, nm	D_{max}, nm
Sep	311.4	0.351	0.265	0.126	6.63	4.00
Sep–ZrI	337.3	0.340	0.236	0.135	6.48	4.00
Sep–ZrII	352.2	0.398	0.306	0.135	6.47	4.00

Specific surface area was increased by the zirconium modification of the Sep. Values of D_{max} and D_{sr} are almost the same for sample before and samples after modification, which was probably the retention of the basic sepiolite structure. The increase in S_{BET} might be attributed to the fact that the loaded zirconium oxide particles on the sepiolite surface are nanosized (Figure 3). Previous studies have shown [40] that amorphous ZrO_2, which is obviously present in Sep-ZrI and Sep-ZrII, have large surface area, approximately 380 m^2/g. The specific surface area and total pore volume were higher for the Sep-ZrII, *i.e.* the higher content and probably more homogeneous deposition of zirconium oxide caused the higher surface area. The increase in S_{BET} was also demonstrated in the case of zirconia-modification of lingo cellulosic butanol residue [41] and zeolite [42].

The results of the pH_{pzc} determination are shown in Figure 4. It can be noticed from the dependence $pH_f = f(pH_i)$ that the curves for all three concentrations of KNO_3 coincide, which indicates that the ions of this electrolyte (K^+ and NO_3^-) are not specifically adsorbed on the samples, meaning that KNO_3 is an inert electrolyte for the Sep-ZrI and Sep-ZrII. According to the pH value of the plateau, the pH_{pzc} of both samples is 7.0±0.1.

The pH_{pzc} of natural sepiolite was 7.4 ± 0.1 [29]. Stankovic and authors [39] reported values of 6.6±0.1 and 6.9±0.1 for the pH_{pzc} of the amorphous zirconium oxides, determined in NaCl and $NaNO_3$ solutions. The pH_{pzc} of zirconium (hydr)oxide reported in the literature by other authors were in

Preprints (www.preprints.org) | NOT PEER-REVIEWED | Posted: 6 June 2023 doi:10.20944/preprints202306.0365.v1

range 6.7-6.9 [43,44]. The fact that the sepiolites/ZrO_2 composites had lower values of pH_{pzc} than the Sep indicates that the surface of the modified sepiolites has gained acidity as a consequence of the presence of zirconium oxide, *i.e.* Zr-OH groups.

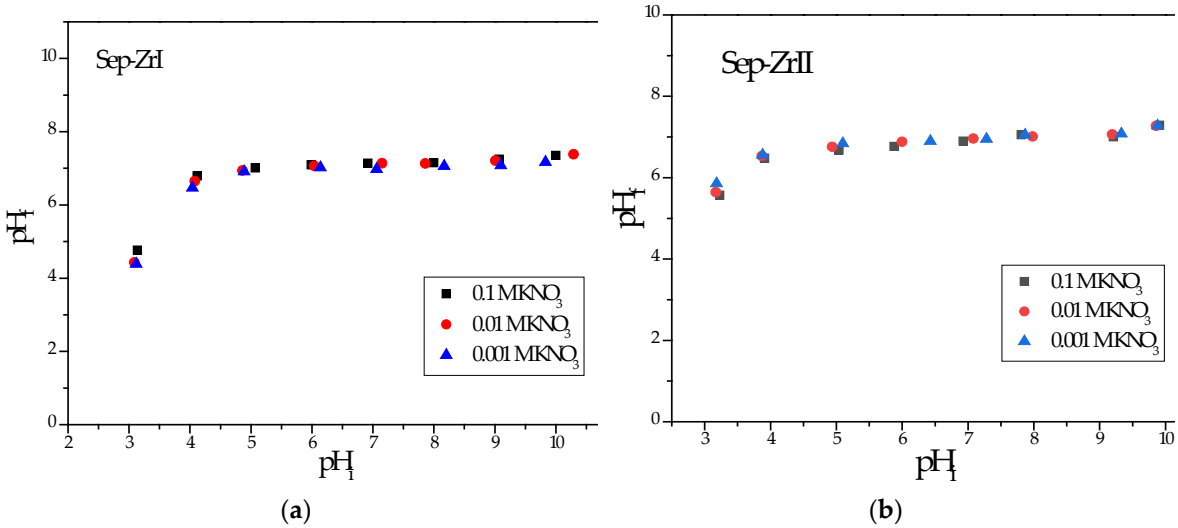

Figure 4. pH_f vs. pH_i during the equilibration of (**a**) Sep-ZrI and (**b**) Sep-ZrII with KNO_3 solutions.

3.2. Adsorption

3.2.1. Effect of solution pH

It was found that the adsorption of phosphates is quite dependent on the pH of the starting solutions (Figure 5a) and that the maximum phosphate adsorption occurred at pH_i= 3. When the pH_i increased from 3 to 10, the adsorption capacities of both SEP-ZrI and SEP-ZrII constantly decreased.

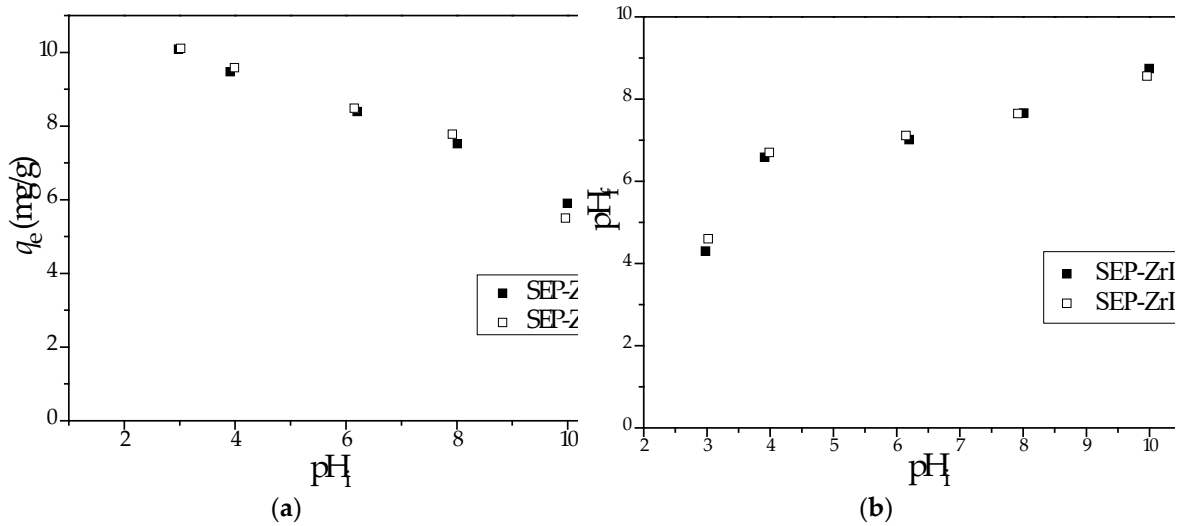

Figure 5. (**a**) Effect of pH_i on phosphate adsorption onto Sep-ZrI and Sep-ZrII; (**b**) final solution pH after phosphate adsorption (pH_f) onto Sep-ZrI and Sep-ZrII.

The pH of the solution affects the type of phosphate species in aqueous solutions and the charge of functional groups on the adsorbent surface. In the investigated solution pH range (pH 3 to 10), the dominant species of phosphate in the solutions are $H_2PO_4^-$ and HPO_4^{2-}. Low solution pH is beneficial for the protonation of the adsorbent surface, which could enhance the electrostatic attraction between the adsorbent surface and the phosphate anions to facilitate the phosphate adsorption. With an increase in pH value, the proportion of ions with a higher negative charge (HPO_4^{2-}) increases, while the positive charge on the surface decreases [7,10], which lead to a decrease in the electrostatic attraction between the phosphate anion and adsorbent and inhibits phosphate adsorption. As the pH

Preprints (www.preprints.org) | NOT PEER-REVIEWED | Posted: 6 June 2023 doi:10.20944/preprints202306.0365.v1

of the solution exceeds pH_{pzc} [7,10], the surface becomes negatively charged and the charge increases with increasing pH. Thus, the Coulomb repulsion between the phosphate anion and the negatively charged surface of the modified sepiolites leads to a further decrease in the phosphate adsorption capacity.

At $pH_i<pH_{pzc}$, the equilibrium pH values (pH_f) increased (Figure 5b), but were below the pH_{pzc} value. This can be assigned to a protonation of the functional groups on the SEP-ZrI and SEP-ZrII samples (Eq. 3), and the protonated positively charged groups can attract phosphate anions (Eq. 4 and 5.):

$$Zr\text{-}OH + H^+ = Zr\text{-}OH_2^+ \quad (3)$$

$$Zr\text{-}OH_2^+ + H_2PO_4^- = (Zr\text{-}OH_2^+)(H_2PO_4^-) \quad (4)$$

$$2\,Zr\text{-}OH_2^+ + HPO_4^{2-} = (Zr\text{-}OH_2)_2^{2+}(HPO_4^{2-}) \quad (5)$$

At $pH_i>pH_{pzc}$, the pH_f values were lower than pH_i, but above the pH_{pzc} value. This can be explained by the release of H^+ into solution due to the ionization of the Zr-OH groups and the negatively charged $Zr\text{-}O^-$ groups are formed.The ratio of the number of groups $Zr\text{-}O^-$ and Zr-OH increased with the pH incensement. Having in mind electrostatic repulsion between phosphate anions and negatively charged surface groups, the adsorption mechanism of the Sep-ZrI and Sep-ZrII at $pH>pH_{pzc}$ can be explained by the exchange of $H_2PO_4^-$ and $HPO_4^{2-}$with OH groups from Zr-OH on the adsorbent surface, *i.e.* by the formation of inter-sphere complexes (Eq. 6 and 7). These complexes are also formed at $pH <pH_{pzc}$.

$$Zr{-}\,OH + H_2PO^{4-} \rightarrow Zr(H_2PO_4) + OH^- \quad (6)$$

$$2Zr\text{-}OH + HPO_4^{2-} = Zr_2(HPO_4) + 2\,OH^- \quad (7)$$

The mechanism for phosphate adsorption onto ZrO_2 has been investigated in previous investigations, showing that the replacement of the hydroxyl group bound to zirconium (Zr-OH) with phosphate and the formation of the Zr-O-P inner-sphere complex are the main mechanism for phosphate adsorption onto ZrO_2 at a solution pH above pH_{pzc} [17,45].

3.2.2. Adsorption isotherms

Adsorption isotherms and fitting of the experimental data with the Freundlich and Langmuir nonlinear models are given in Figure 6. The adsorption isotherms constants are summarized in Table 4.

Preprints (www.preprints.org) | NOT PEER-REVIEWED | Posted: 6 June 2023 doi:10.20944/preprints202306.0365.v1

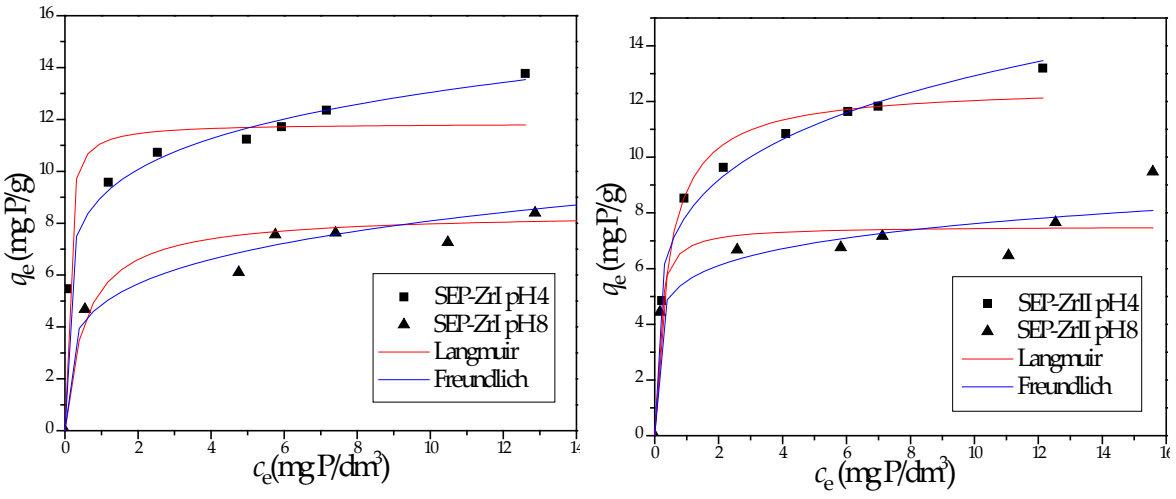

Figure 6. Adsorption isotherms for phosphate onto Sep-ZrI (**a**) and Sep-ZrII (**b**) at pH of 4 ± 0.1 and 8 ± 0.1.

According to the adsorption isotherms, the adsorption capacities of both samples are higher at pH_i=4 ± 0.1 than at pH_i=8 ± 0.1, as expected based on the results at Fig. 5a. Bearing in mind that the adsorption capacity of sepiolite for phosphates is practically equal to zero, the capacity of the Sep-ZrI and Sep-ZrII is the result of the presence of the Zr- phase. The capacity of the Sep-ZrI and Sep-ZrII was almost the same at both pH_i, regardless of the somewhat larger content (Table 1) and better dispersion (Figure 3) of the Zr-phase in Sep-ZrII.

According to the correlation coefficients R^2 (Table 3), the Freundlich model describes phosphate adsorption on both samples and both pH_i values better than the Langmuir model. The Freundlich model assumes adsorption on a heterogeneous surface consisting of non-identical and energetically non-uniform sites. Thus, phosphate is adsorbed on the functional groups of different energies at the surface of Zr-phase, probably protonated and non-protonated Zr-OH.

Table 3. Adsorption equilibrium constants obtained from Langmuir and Freundlich isotherms for the adsorption of phosphate onto Sep-ZrI and Sep-ZrII.

Sample	pH_i	**Langmuir isotherm** $q_e = \frac{q_m K_L c_e}{1 + K_L c_e}$			**Freundlich isotherm** $q_e = K_f \cdot c_e^{1/n}$		
		q_m mg/g	K_L dm^3/mg	R^2	$1/n$	K_f (mg/g)(dm^3/mg)$^{1/n}$	R^2
Sep-ZrI	4.0	11.85	14.45	0.935	0.160	9.01	0.996
	8.0	8.47	1.81	0.905	0.221	4.85	0.957
Sep-ZrII	4.0	12.55	2.32	0.982	0.212	7.93	0.988
	8.0	7.52	8.41	0.897	0.137	5.56	0.932

q_m (mg/g)- the maximum adsorption capacity, K_L - the Langmuir constant related to the energy of adsorption (dm^3/mg), K_f - the Freundlich constant related to the adsorption capacity (mg$^{(1-1/n)}$ dm$^{3/n}$/g), n - the dimensionless adsorption intensity parameter.

The value of the K_F coefficient indicates the adsorption capacity of the adsorbent. An increase in the coefficient in the sequence Sep-ZrI, pH_i 4 ± 0.1 > Sep-ZrII, pH_i 4 ± 0.1 > Sep-ZrII, pH_i 8 ± 0.1 > Sep-ZrI, pH_i 8 ± 0.1, indicates an increase in adsorption capacity, which indicates that the highest capacity of the Sep-ZrI sample is at pH_i = 4 ± 0.1, and the lowest capacity of the Sep-ZrI sample is at pH_i = 8. Nevertheless, the difference between the samples for the same pH_i is small, indicating a slight difference in adsorption capacity, as already stated.

Preprints (www.preprints.org) | NOT PEER-REVIEWED | Posted: 6 June 2023 doi:10.20944/preprints202306.0365.v1

A comparison of phosphate adsorption by the Sep-Zr samples to other adsorbents containing Zr is presented in Table 4.

Table 4. The phosphate adsorption capacities of Sep-ZrI and Sep-ZrII in comparison to other adsorbents containing Zr.

Adsorbent	Capacity	pH	Reference
Zirconia-functionalized graphite oxide	16.45 mg PO_4^{3-}/g	6	27
ZrO_2/Fe_3O_4 composite	59.9 mg PO_4^{3-}/g	4	46
Amorphous-ZrO_2	99.01 mg PO_4^{3-}/g	6.2	11
Zirconium-modified bentonite	8.90 mg PO_4^{3-}/g	7	17
Zirconium (IV) loaded cross-linked chitosan particles	71.68 mg PO_4^{3-}/g	3	21
La-Zr modified magnetite	49.1 mg PO_4^{3-}/g	2	47
Magnetic zirconium-based metal–organic frameworks	12.82 mg P/g	6.5	1
Zirconium-modified zeolite	10.2 mg P/g	7	14
Zirconium(IV) loaded lignocellulosic butanol residue	8.75 mg P/g	6	41
Sep-Zr I	13.5 mg P/g (41.4 mg PO_4^{3-}/g)	4	This study
Sep-Zr I	9.8 mg P/g (30.0 mg PO_4^{3-}/g)	8	This study
Sep-Zr II	13.2 mg P/g (40.45 mg PO_4^{3-}/g)	4	This study
Sep-Zr II	9.4 mg P/g (28.8 mg PO_4^{3-}/g)	8	This study

The phosphate adsorption capacities of the materials used in this work are comparable to the capacity of other similar materials obtained by the deposition of ZrO_2 onto different supports. Compared to amorphous ZrO_2, all the presented adsorbents have smaller capacity, which indicates that ZrO_2 is active phase for the phosphate adsorption. It should be emphasized that Sep-ZrI and Sep-ZrII have relatively high adsorption capacities at $pH_i = 8 \pm 0.1$, which is the pH of natural waters.

3.2.3. Phosphate adsorption kinetics

Figures 7 and 8 show the effect of equilibration time on the quantities of adsorbed phosphates on Sep-ZrI and Sep-ZrII, at different pH_i and different initial concentrations.

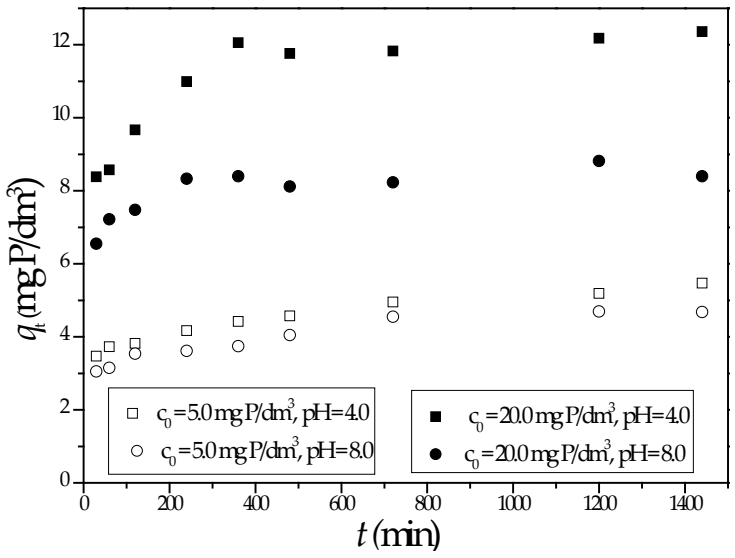

Figure 7. Effect of contact time on the adsorbed amount of phosphate onto Sep-ZrI at pH_i 4 ± 0.1 and 8 ± 0.1.

Preprints (www.preprints.org) | NOT PEER-REVIEWED | Posted: 6 June 2023 doi:10.20944/preprints202306.0365.v1

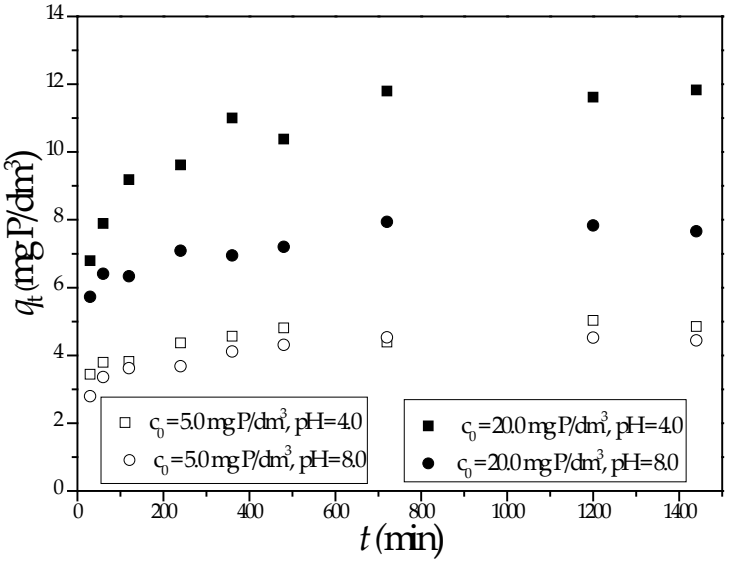

Figure 8. Effect of contact time on the adsorbed amount of phosphate onto Sep-ZrII at pH_i 4 ± 0.1 and 8 ± 0.1.

Examination of phosphate adsorption kinetics at different pH values and initial concentrations confirms that the adsorption capacity of both samples is higher at pH_i = 4 ± 0.1 than at pH_i = 8 ± 0.1. Phosphate adsorption in all cases takes place in two stages: first, in which the number and availability of sites for adsorption are large, so the driving force for adsorption is also large and the adsorption takes place at a high speed; and second, in which adsorption takes place more slowly because the number of available sites for adsorption is reduced [48]. Table 5 shows the kinetic parameters and correlation coefficients for pseudo-first, pseudo-second-order and intraparticle kinetic models.

Table 5. Kinetic parameters of pseudo-first, pseudo-second-order and intraparticle model fitting for the adsorption of phosphate on Sep-ZrI and Sep-ZrII, from solutions of different concentrations.

Adsorbent/pH	Model								
	Pseudo – first			Pseudo – second			Intraparticle		
	k_1 (1/min)	q_e (mg/g)	R^2	k_2 (g/mg·min)	q_e (mg/g)	R^2	k_i (mg/g·min$^{1/2}$)	C (mg/g)	R^2
Sep-ZrI c_0 = 5.0 mg P/dm^3, pH 4	0.0017	1.97	0.992	0.0030	5.52	0.996	0.0598	3.22	0.988
Sep-ZrI c_0 = 20.0 mg P/dm^3, pH 4	0.0026	2.80	0.752	0.0029	12.51	0.999	0.2842	6.60	0.989
Sep-ZrI c_0 = 5.0 mg P/dm^3, pH 8	0.0029	1.95	0.962	0.0036	4.85	1.00	0.0648	2.68	0.950
Sep-ZrI c_0 = 20.0 mg P/dm^3, pH 8	0.0009	1.20	0.447	0.0036	8.55	0.988	0.1368	5.99	0.939
Sep-ZrII c_0 = 5.0 mg P/dm^3, pH 4	0.0014	1.10	0.651	0.0067	4.97	0.997	0.0807	3.05	0.975
Sep-ZrII c_0 = 20.0 mg P/dm^3, pH 4	0.0034	3.90	0.621	0.0020	12.09	0.999	0.2858	5.54	0.952
Sep-ZrII c_0 = 5.0 mg P/dm^3, pH 8	0.0031	1.09	0.630	0.0071	4.58	1.00	0.0743	2.63	0.930
Sep-ZrII c_0 = 20.0 mg P/dm^3, pH 8	0.0017	1.75	0.842	0.0054	7.87	0.999	0.0880	5.46	0.910

k_1- pseudo first-order rate constant(1/min), q_t - adsorption capacity at time t (mg/g), q_e - adsorption capacity at equilibrium (mg/g), k_2 - pseudo-second order rate constant (g/mg min), q_t - adsorption capacity at time t mg/g),

Preprints (www.preprints.org) | NOT PEER-REVIEWED | Posted: 6 June 2023 doi:10.20944/preprints202306.0365.v1

q_e - adsorption capacity at equilibrium(mg/g), k_i - intraparticle diffusion rate constant (mg/g $min^{1/2}$) *C* – intercept at the ordinate, related to the boundary layer thickness (mg/g).

Based on the results given in Table 5, it can be seen that the phosphate adsorption process in all cases can be best described by a pseudo-second-order kinetic model, which can indicate that the slowest adsorption step may be chemisorption, which involves the exchange or sharing of electrons between the adsorbent and the adsorbate. The pseudo-second-order model includes all steps of adsorption: external film (boundary layer) diffusion, internal particle diffusion and adsorption. The third step is assumed rapid and thus the slowest step would be either film diffusion or pore diffusion.

To determine which step in the adsorption of phosphate was the slowest, the intra-particle diffusion model was applied to the results. In all cases, the dependences q_t *vs.* $t^{1/2}$ were consisted of two linear portions (the dependences are not shown) where the first indicated intra-particle diffusion and the second was for equilibrium. The first part did not pass through the origin, which means that intra-particle diffusion was involved in the adsorption, but was not the rate-limiting step.

3.2.4. ATR-FTIR study

The phosphate adsorption mechanism was further investigated by FTIR spectroscopy. Figure 9. shows the FTIR spectra of the Sep, the Sep-ZrI before and after phosphate adsorption, and the Sep-ZrII.

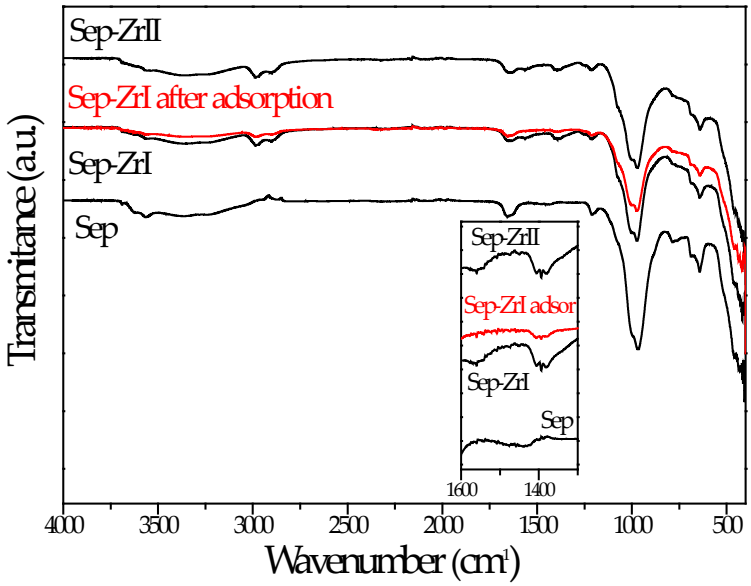

Figure 9. ATR-FTIR spectra of samples Sep, Sep-ZrI, Sep-ZrI after phosphate adsorption and Sep-ZrII.

The ATR-FTIR spectra of the modified samples (Figure 9) were generally similar to that of natural sepiolite, confirming that the modified materials had maintained the basic structure of sepiolite. Three regions indicative for sepiolite were observed in Figure 10: i) bands in the 4000–3000 cm^{-1} range corresponding to the vibrations of the Mg–OH group (3690 cm^{-1}), bound water coordinated to magnesium in the octahedral sheet (3570 cm^{-1}) and zeolitic water in the channels (at 3422 cm^{-1}); ii) a band at 1658 cm^{-1} due to the vibration of zeolitic water; and iii) bands in the 1200–400 cm^{-1} range characteristic of silicate: bands centered at 1002 and 460 cm^{-1} due to Si–O–Si vibration; bands at 1205 and 970cm^{-1}due to Si–O bonds; a band at 437 cm^{-1} originating from octahedral–tetrahedral bonds (Si–O–Mg bonds), and bands at 688 and 642 cm^{-1} corresponding to vibrations of the Mg–OH bond.

After modification, weak bands at 1562 $cm^{-1}$and 1385 cm^{-1} appeared which can be assigned to the vibration of Zr–OH [40]. After phosphate adsorption onto Sep-ZrI, the intensity of these bands

Preprints (www.preprints.org) | NOT PEER-REVIEWED | Posted: 6 June 2023 doi:10.20944/preprints202306.0365.v1

significantly decreased, which probably indicates phosphate adsorption and the replacement of the Zr-OH bond by Zr-OP bond. The characteristic band that corresponds to the P–O bond at 960 cm^{-1} cannot be clearly seen [40], because it is overlapped with the band for Si-O bonds.

3.2.5. XPS Analysis

In order to further clarify the mechanism of the adsorption, XPS analysis of the Sep-ZrI before and after adsorption was conducted and the results are shown in Figure 10.

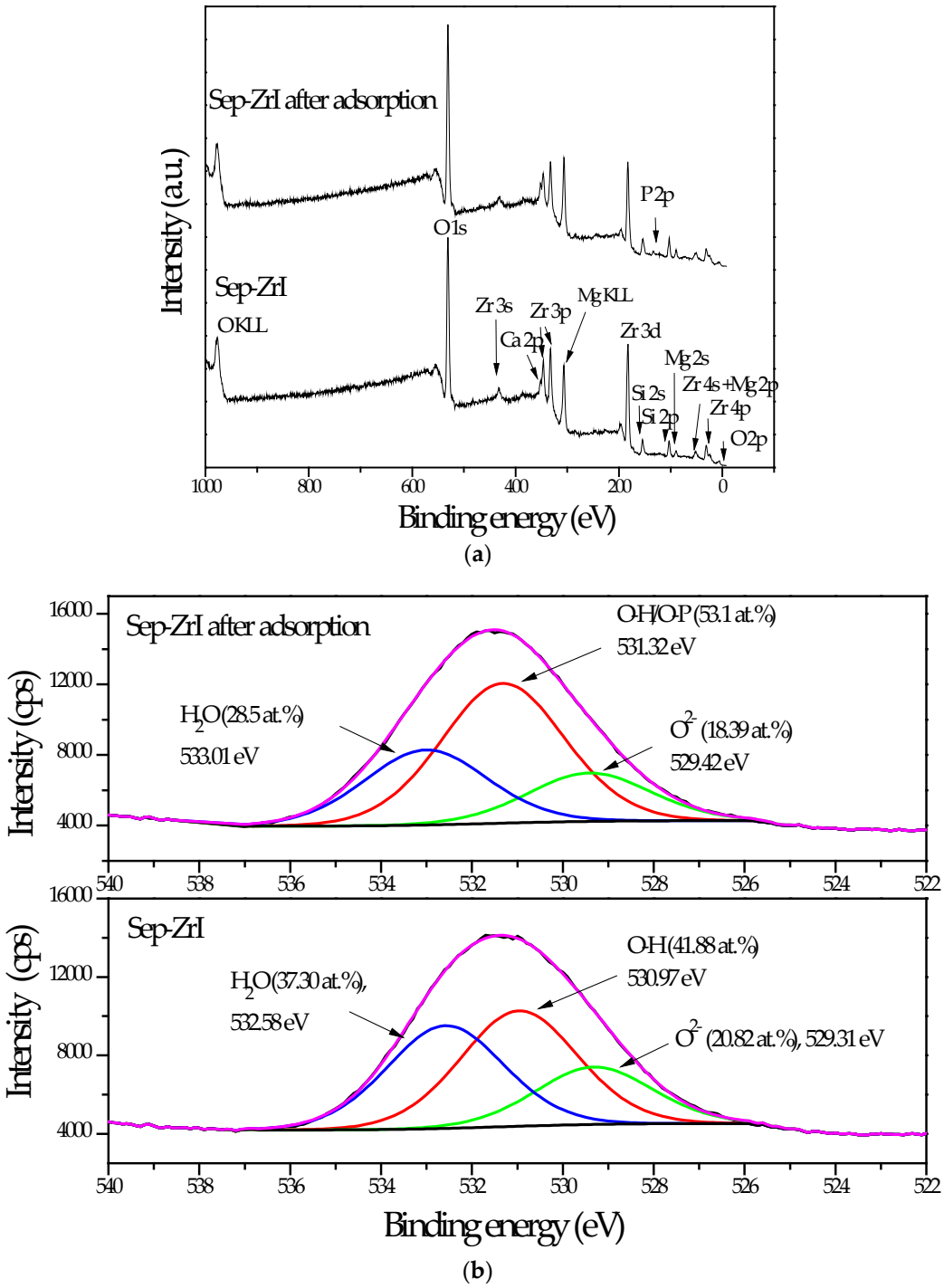

Figure 10. XPS spectra of Sep-ZrI (**a**) full-spectrum scanning; and (**b**) O1s orbital spectra of Sep-ZrI before and after adsorption.

The presence of distinguished sharp peaks of Mg 1s, Mg 2s, Si 2s, Si 2p, Zr 3s, Zr 3p, Zr 3d and O 1s in the XPS full-scan spectrum of Sep-ZrI (Figure 10a) suggests the presence of sepiolite and Zr-

Preprints (www.preprints.org) | NOT PEER-REVIEWED | Posted: 6 June 2023 doi:10.20944/preprints202306.0365.v1

phase in the sample. A new peak of P-2p appeared in the wide-scan spectrum of the Sep-ZrI after phosphate adsorption, indicating that phosphate has been adsorbed onto the surface of the Sep-ZrI. The P2p binding energy of P-loaded Sep-ZrI was located at 133.6 eV, which is a slightly higher value then the P2p binding energy of $NaH_2PO_4 \cdot 2H_2O$ reference sample [45] (132.0–132.9 eV). This difference can be explained by the formation of strong specific interactions between phosphate and adsorbent rather than the formation of non-specific electrostatic attraction between the adsorbent and phosphate [45].

The O1s peak of the sample before adsorption can be resolved in three contributions: lattice oxygen (O^{2-}), oxygen from surface hydroxyl groups (-OH), and oxygen from adsorbed water (H_2O) (Figure 10b). In the case of the sample after adsorption, the peak was also fitted in three contributions, but their fractions are changed: the fraction of oxygen from surface hydroxyl groups increased and the other two proportionally decreased. This incensement can be explained by the replacement of OH groups (from Zr-OH) with HPO_4^{2-} or $H_2PO_4^-$, where upon O-H bond from Zr-OH is replaced by O-P bond. At the same time, some new O-H groups are included on the surface withHPO_4^{2-} or $H_2PO_4^-$. Therefore, the contribution of oxygen from surface OH groups in O1s peak corresponds actually to the oxygen from O-P and O-H groups. These findings confirm the formation of inner-sphere complexes as the mechanism of phosphate adsorption onto Sep-ZrI sample. In addition, positions of all three contributions shifted slightly to higher binding energies, illustrating a change in the oxygen environment due to the presence of phosphorus.

3.2.6. Desorption

In order to examine the stability and potential regeneration of the sepiolite/ZrO_2 loaded by phosphate (phosphate adsorbed at pH 4 ± 0.1 and 8 ± 0.1) desorption was conducted in NaOH solution, concentration of 0.1 M. The dependences of desorption efficiency on contact time are shown in Figure 11.

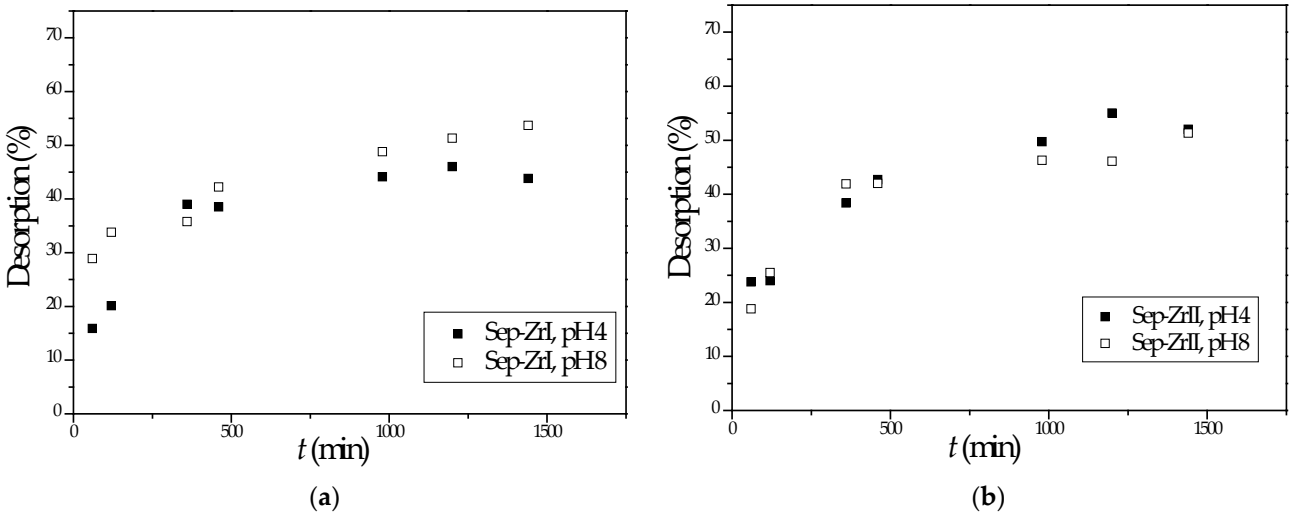

Figure 11. Desorption of phosphate from the saturated Sep-ZrI (**a**) and Sep-ZrII (**b**).

The presented results (Figure 11) indicate slow desorption and the maximum percentage of desorption is approximately 50% after 24 h for all the samples. Obviously, P adsorption on the sepiolite/ZrO_2 is not completely reversible. It can be supposed that the easily desorbed phosphates were bonded in the outer-sphere complexes, while the slow-releasing phosphates were in the inner-sphere complexes. Due to the slow release of phosphorus, the zirconium-enriched sepiolites used for phosphate adsorption might be applied as artificial fertilizers. Due to the controlled and dosed release of phosphorus, this could be one of the solutions for the soil's phosphorus deficit.

5. Conclusions

The sepiolite/amorphous ZrO_2 composites were successfully prepared and used for phosphate removal from aqueous solutions. Although zirconium propoxide in toluene was used to provide a molecular level dispersion of ZrO_2 functionality, aggregates of nanoparticles were also observed by FESEM, so in the sample synthesized at a lower temperature. In addition, a higher temperature of synthesis for a shorter time (95 °C, 4 h in comparison to room temperature, 24 h) provided a slightly higher content of ZrO_2, but the capacities of both composites at both investigated pH values were practically the same. As expected, capacities were lower at higher pH, but it is important that the composites have a significantly large capacity (~ 10 mg P/g) at pH close to the pH of natural waters (pH = 8 ± 0.1). The Freundlich isotherm and pseudo-second-order kinetic model fitted well to the obtained adsorption data. XPS and ART-FTIR characterization of the sample before and after adsorption indicated the formation of inner-sphere complexes as the mechanism of phosphate uptake by the composites. Desorption studies confirmed the formation of inner-sphere complexes, from which the phosphates were released slowly, but also the formation of other-sphere complexes, from which phosphates were easily desorbed.

Author Contributions: Conceptualization, R.P and S.L; methodology, R.P, S.L and Ž. M.; formal analysis, Ž. M, I. J. Č, Ž.R and S.L.; investigation, Ž. M, I. J. Č, Ž.R and S.L.; writing—original draft preparation, Ž. M; writing—review and editing, R.P and S.L; supervision, R.P, Đ. J. and S. C. All authors have read and agreed to the published version of the manuscript.

Funding: This work was supported by the Ministry of Science, Technological Development and Innovation of the Republic of Serbia through the project contracts No. 451-03-47/2023-01/200135, 451-03-47/2023-01/200287 and 451-03-47/2023-01/200026.

Data Availability Statement: Data is available upon request.

Conflicts of Interest: The authors declare no conflict of interest.

References

1. Liu, T.; Zheng, S.; Yang, L. Magnetic zirconium-based metal–organic frameworks for selective phosphate adsorption from water, *J. Colloid Interf. Sci.* **2019**, *552*, 134–141.
2. Mitrogiannis, D.; Psychoyou, M.; Baziotis, I.; Inglezakis, V.J.; Koukouzas, N.; Tsoukalas, N.; Palles, D.; Kamitsos, E.; Oikonomou, G.; Markou, G. Removal of phosphate from aqueous solutions by adsorption onto $Ca(OH)_2$ treated natural clinoptilolite, *Chem. Eng. J.* **2017,** *320*, 510–522.
3. Xiong, W.; Tong, J.; Yang, Z.; Zeng, G.; Zhou, Y.; Wang, D.; Song, P.; Xu, R.; Zhang, C.; Cheng, M. Adsorption of phosphate from aqueous solution using iron-zirconium modified activated carbon nanofiber: Performance and mechanism, *J. Colloid Interf. Sci.* **2017**, *493*, 17–23.
4. Goscianska, J.; Ptaszkowska-Koniarz, M.; Frankowski, M.; Franus, M.; Panek, R.; Franus, W. Removal of phosphate from water by lanthanum-modified zeolites obtained from fly ash, *J. Colloid Interf. Sci.* **2018**, *513*, 72–81.
5. Han, C.; Lalley, J.; Iyanna, N.; Nadagouda, M.N. Removal of phosphate using calcium and magnesium-modified iron based adsorbents, *Mater. Chem. Phys.* **2017**, *198*, 115-124.
6. Fu, H.; Yang, Y.; Zhu, R.; Liu, J.; Usman, M.; Chen, Q.; He, H. Superior adsorption of phosphate by ferrihydrite-coated and lanthanum-decorated Magnetite, *J. Colloid Interf. Sci.* **2018**, *530*, 704–713.
7. Wu, B.; Fang, L.; Fortner, J.D.; Guan, X.; Lo, I.M.C. Highly efficient and selective phosphate removal from wastewater by magnetically recoverable $La(OH)_3/Fe_3O_4$ nanocomposites, *Water Res.* **2017,** *126*, 179-188.
8. Xu, Y.; Hong, H.; Yang, F.; Zhang, L.; Xu, J.; Dou, L.; Hao, Y.; Qian, G.; Zhou, J. Removal behaviors and mechanisms of orthophosphate and pyrophosphate by calcined dolomite with ferric chloride assistance, *Chemosphere* **2019**, *235*, 1015-1021.
9. Ya, W.; Zhao, H.D.L.; Liud, Q.; Tao, Q.; Zhua, Y.; Yanga, J.; Zhang, Y.M. Kinetics, isotherm, thermodynamic, and adsorption mechanism studies of $La(OH)_3$-modified exfoliated vermiculites as highly efficient phosphate adsorbents, *Chem. Eng. J.* **2014,** *236*, 191-201
10. Liua, R.; Chia, L.; Wanga, X.; Suia, Y.; Wang, Y.; Arandiyan, H. Review of metal (hydr)oxide and other adsorptive materials for phosphate removal from water, *J. Environ. Chem. Eng.* **2018,** *6*, 5269–5286
11. Su, Y.; Cui, H.; Li, Q.; Gao, S.; Shang, J.K. Strong adsorption of phosphate by amorphous zirconium oxide nanoparticles, *Water Res.* **2013**, *47*, 5018-5026.
12. Liu, H.; Sun, X.; Yin, C.; Hu, C. Removal of phosphate by mesoporous ZrO_2, *J. Hazard. Mater.* **2008**, *151*, 616-622.
13. Tao, Y.; Liu, S.; Dong, S.; Wang, C.; Qu, T.; Li, S.; Lib, L.; Ma, Z. An in situ grown amorphous ZrO_2 layer on zeolite for enhanced phosphate adsorption, *RSC Adv.* **2022**, *12*, 16751–16762.

14. Yanga, M.; Lina, J.; Zhana, Y.; Zhang, H. Adsorption of phosphate from water on lake sediments amended with zirconium-modified zeolites in batch mode, *Ecol. Eng.* **2014**, *71*, 223–233.
15. Nguyen, T.A.H.; Ngo, H.H.; Guo, W.S.; Zhou, J.L.; Wang, J.; Liang, H.; Li, G. Phosphorus elimination from aqueous solution using 'zirconium loaded okara' as a biosorbent. *Bioresource Technol.* **2014**, *170*, 30–37.
16. Nguyen, T.A.H.; Ngo, H.H.; Guo, W.S.; Pham, T.Q.; Li, F.M.; Nguyen, T.V.; Bui, X.T. Adsorption of phosphate from aqueous solutions and sewage using zirconium loaded okara (ZLO): fixed-bed column study, *Sci. Total Environ.* **2015**, *523*, 40–49.
17. Lin, J.; Jiang, B.; Zhan, Y. Effect of pre-treatment of bentonite with sodium and calcium ions on phosphate adsorption onto zirconium-modified bentonite, *J. Environ. Manage.* **2018**, *217*, 183-195.
18. Tang, Y.; Zong, E.; Wan, H.; Xu, Z.; Zheng, S.; Zhu, D. Zirconia functionalized SBA-15 as effective adsorbent for phosphate removal, *Micropor. Mesopor. Mat.* **2012**, *155*, 192–200.
19. Padungthon, S.; German, M.; Wiriyathamcharoen, S.; SenGupta, A.K. Polymeric anion exchanger supported hydrated Zr(IV) oxide nanoparticles: A reusable hybrid sorbent for selective trace arsenic removal, *React. Funct.Polym.* **2015**, *93*, 84-94.
20. Chena, L.; Zhaoa, X.; Pana, B.; Zhang, W.; Huaa, M.; Lv, L.; Zhanga, W. Preferable removal of phosphate from water using hydrous zirconium oxide-based nanocomposite of high stability, *J. Hazard Mater.* **2015**, *284*, 35–42.
21. Liu, Q.; Hu, P.; Wang, J.; Zhang, L.; Huang, R. Phosphate adsorption from aqueous solutions by Zirconium (IV) loaded cross-linked chitosan particles, *J. Taiwan. Inst. Chem. E.* **2015**, *000*, 1–9.
22. Marjanović, V.; Lazarević, S.; Janković-Častvan, I.; Jokić, B.; Janaćković, Đ.; Petrović, R., Adsorption of chromium (VI) from aqueous solutions onto amine- functionalized natural and acid-activated sepiolites, *Appl. Clay. Sci.* **2013,** *80-81*, 202-210.
23. Zhang, Z.; Liu, T.; Wu, D. Facile synthesis of hydrous zirconia-impregnated chitosan beads as a filter medium for efficient removal of phosphate from water, *Cellulose* **2022**, *29*, 8749–8768.
24. Zhan, Y.; Zhang, H.; Lin, J.; Zhang, Z.; Gao, J. Role of zeolite's exchangeable cations in phosphate adsorption onto zirconium-modified zeolite, *J. Mol. Liq.* **2017**, *243*, 624–637.
25. Shao, Y.; Li, J.; Fang, X.; Yang, Z.; Qu, Y.; Yang, M.; Tan, W.; Li, G.; Wang, H. Chemical modification of bamboo activated carbon surface and its adsorption property of simultaneous removal of phosphate and nitrate, *Chemosphere* **2022**, *287*, 132118.
26. Shana, S.; Tanga, H.; Zhaoa, Y.; Wanga, W.; Cuia, F. Highly porous zirconium-crosslinked graphene oxide/alginate aerogel beads for enhanced phosphate removal, *Chem. Eng. J.* **2019**, *359*, 779–789.
27. Zong, E.; Wei, D.; Wan, H.; Zheng, S.; Xu, Z.; Zhu, D. Adsorptive removal of phosphate ions from aqueous solution using zirconia-functionalized graphite oxide, *Chem. Eng. J.* **2013,** *221*, 193-203.
28. Marjanović, V.; Lazarević, S.; Janković-Častvan, I.; Potkonjak, B.; Janaćković, Đ.; Petrović, R. Chromium (VI) removal from aqueous solutions using mercaptosilane functionalized sepiolites, *Chem. Eng. J.* **2011**, *166*, 198-206.
29. Lazarević, S.; Janković-Častvan, I.; Jovanović, D.; Milonjić, S.; Janaćković, Đ.; Petrović, R. Adsorption of Pb^{2+}, Cd^{2+} and Sr^{2+} ions onto natural andacid-activated sepiolites, *Appl. Clay. Sci.* **2007**, *37*, 47–57.
30. Rouquerol, F.; Rouquerol, J.; Sing, K. Adsorption by Powders and Porous Solids, Academic Press, **1975**.
31. Barrett, E.P.; Joyner, L.G.; Halenda, P.P. The determination of pore volume and area distributions in porous substances. I. Computations from nitrogen isotherms, *J. Am. Chem. Soc.* **1951**, *73*, 373-380.
32. Lippens, B.C.; De, Boer J.H. Studies on pore systems in catalysts V. The t method, *J. Catal.*, **1965**, *4*, 319-323.
33. Waseem, M.; Mustafa, S.; Naeem, A.; Koper, G.J.M.; Shah, K.H. Cd^{2+}sorption characteristics of iron coated silica, *Desalinatio*, **2011**, *277*, 221-226.
34. Langmuir, I. The adsorption of gases on plane surfaces of glass, mica and platinum, *J. Am. Chem. Soc.* **1918**, *40*, 1361–1403.
35. Freundlich, H. Concerning adsorption in solutions, *Zeitschriftfür Physikalische Chemie*,**1906**, *57*, 385–470.
36. Lagergren, S. About the theory of so-called adsorption of soluble substances, *K. Sven.Vetenskapsakad.Handl.***1989** , *24*, 1–39.
37. Ho, Y.S.; McKay, G. Pseudo-second order model for sorption processes, *Process Biochem.* **1999**, *34*, 451–465.
38. Weber, Jr. W.J.; Morris, J.C. Kinetics of adsorption on carbon from solution, *J. Sanit. Eng. Div. ASCE* **1963**, *89*, 31–59.
39. Stankovic, J.B.; Milonjic, S.K.; Zec, S.P. The influence of chemical and thermal treatment on the point of zero charge of hydrous zirconium oxide. *J. Serb. Chem.Soc.* **2013**, *78*, 987–995.
40. Song, L.; Li, J.; Zhou, H.; Lin, Y.; Ding, H.; Huang, Y.; Zhang, P.; Lai, X.; Liu, G.; Fan, Y. Zirconia nano-powders with controllable polymorphs synthesized by a wet chemical method and their phosphate adsorption characteristics & mechanism, *Ceram Int.* **2022**, *48*, 6591–6599.
41. Zong, E.; Liu, X.; Jiang, J.; Fu, S.; Chu, F. Preparation and characterization of zirconia-loaded lingo cellulosic butanol residue as a biosorbent for phosphate removal from aqueous solution, *Appl. Surf. Sci.* **2016**, *387*, 419–430.

42. Lin, J.; Zhang, Z.; Zhan, Y. Effect of humic acid preloading on phosphate adsorption onto zirconium-modified zeolite, *Environ. Sci. Pollut. Res.* **2017**, *24*, 12195–12211.
43. Kosmulski, M. The Significance of the Points of Zero Charge of Zirconium (Hydr)Oxide Reported in the Literature, *J. Dispersion Sci. Technol.* **2002**, *23*, 529-538.
44. Pettersson, A.; Marino, G.; Pursiheimo, A.; Rosenholm, J.B. Electrosteric Stabilization of Al_2O_3, ZrO_2, and 3-Y-ZrO_2 Suspensions: Effect of Dissociation and Type of Polyelectrolyte, *J. Colloid Interf. Sci.* **2000**, *228*, 73-81.
45. Lin, J.; He, S.; Wang, X.; Zhang, H.; Zhana, Y. Removal of phosphate from aqueous solution by a novel $Mg(OH)_2/ZrO_2$ composite: Adsorption behavior and mechanism, *Colloids and Surfaces* **2019** , *561*, 301–314.
46. Lee, W.H.; Kim, J.O. Mechanisms and novel performance of ZrO_2/Fe_3O_4 composite for
47. phosphate recovery from wastewater, *Chem. Eng. J.* **2023**, *453*, 139817.
48. Lin, X.; Xie, Y.; Lu, H.; Xin, Y.; Altaf, R.; Zhu, S.; Liu, D. Facile preparation of dual La-Zr modified magnetite adsorbents for efficient and selective phosphorus recovery, *Chem. Eng. J.* **2021**, *413*, 127530.
49. Zhou, K.; Wua, B.; Su, L.; Xin, W.; Chai, X. Enhanced phosphate removal using nanostructured hydrated ferric zirconium binary oxide confined in a polymeric anion exchanger, *Chem. Eng. J.* **2018**, *345*, 640-647.